Load-carrying capacity of welded K-type joints inside floor truss systems

Pooya Saremi, Wei Lu[1], Jari Puttonen, Dan Pada, and Jyrki Kesti

Summary. The load-carrying capacity of a K-type joint inside a floor truss is studied both experimentally and numerically. The joint tested is a scaled-down, isolated joint. The tubular braces, plate chord, and division plate are made of SSAB Domex steel. Comparison of load displacement curves received by finite element analyses with curves obtained from tests confirms that numerical models describe joint behaviour reasonable. The paper demonstrates that joints with high load-bearing capacity can be investigated experimentally by scaling the dimensions of the joint down when testing devices can affect the required capacity of the joint. The results presented can also be used for optimizing failure mechanism of similar joints in practice.

Keywords: welded K-type tube-to-plate joint, long-span steel truss, high strength steel, sustainable steel building

Introduction

The building industry widely uses trusses in floor systems to get benefits of long spans and high strength-to-weight ratio. In recent years, the availability of high-strength steel grades and mass productions of hollow structural steel sections have promoted the application of light-weight trusses with longer spans and increased load-bearing capacities to enhance sustainable construction.

A novel truss-floor system that has been invented and currently used in Finland is shown in Figure 1. The truss has a WQ-beam as its upper chord, square hollow sections as its braces, and a steel plate as its lower chord. The edge truss joint is a K-type joint, which is reinforced by a welded division plate between the two hollow-section braces and the lower chord. No specified rules for designing this type of reinforced K-type joints are available in current version of EN 1993-1-8 [3]. A series of research studies by Jurmu [4], Kadak [5], Saremi [7], and Saremi et.al [8] have been carried out in investigating the joint

---

[1]Corresponding author: wei.2.lu @aalto.fi

behaviour by numerical simulations. However, the results from numerical studies have not been validated by experimental tests.

Saremi et.al [8] has performed parametric studies using finite element (FE) analyses to determine appropriate boundary conditions and optimum brace lengths suitable for experimental tests. The studies have followed common practices to investigate the behaviour of tubular joints as in [1], [2], [6], [13]. Because of the available testing environment and the target to seek the new options for performing the experimental tests, the scaled-down specimens have been designed using similitude theory as in [7]. The test arrangement was designed based on the dimensions of the scaled down joint.

In this paper, the test specimens, the test setup, instrumentations, and the procedure of tests are firstly described. The experimental results are then used to validate the FE model created for the scaled-down, isolated joint tested. The results from the validated FE model are scaled-up to validate FE models developed for the full-scale joint. With this validation procedure, the FE models of scaled-down and full-scale joint can be used in studying the behaviour of the joint.
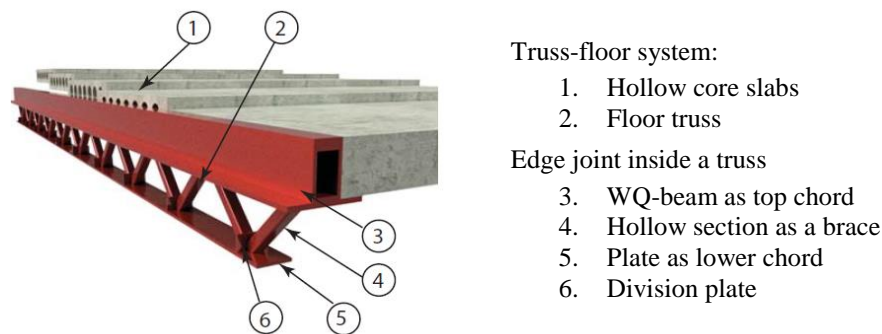

Truss-floor system:
1. Hollow core slabs
2. Floor truss

Edge joint inside a truss
3. WQ-beam as top chord
4. Hollow section as a brace
5. Plate as lower chord
6. Division plate

Figure 1. Details of edge joint inside truss-floor system

Geometrical configuration and material properties of specimens

The geometrical configuration of the specimen is determined based on the results of the numerical parametric studies on the full-scale, isolated joint. The dimensions of the specimens are determined by reducing the dimensions of the full-scale joint using a scale factor of 3.46, which is obtained from the studies in [7]. The final shape of the specimen installed on the testing setup is shown in Figure 2. The specimen has two braces with lengths of four times of their widths, and a chord with length of five times of its width. In order to attach the specimen to the test set-up, end plates are welded to the ends of the chord and the braces. Four test specimens were tested.

The steel of SSAB Domex 420ML was used for manufacturing the chord and the division plate of the joint. The steel grade meets or exceeds the requirements of S420 ML as provided in EN10025-4 [9]. The braces are made of SSAB Domex tube double grade steel. This steel meets or exceeds the requirements of standard EN 10219 [10], [11], and includes two steel grades: S355J2H and S420MH [12]. The test of tensile coupons was carried out to get the values of mechanical properties. The tensile coupons were taken from three weld-free surfaces of the cross-section of tubular braces. Two separate

coupons are prepared from each selected surface. Eight coupons, of which four coupons taken from division plates and four taken from chords, were prepared. Table 1 reports the average values of the measured mechanical properties for the braces, the chord, and the division plate. The measured mechanical properties include yield strength, R_{eh}, ultimate strength, R_m, and ultimate strain at fracture, ε_u. The strain was measured over a gauge length of 50 mm. The electrode used for welds inside the joint is ESAB AristoRod $\phi1.0$.
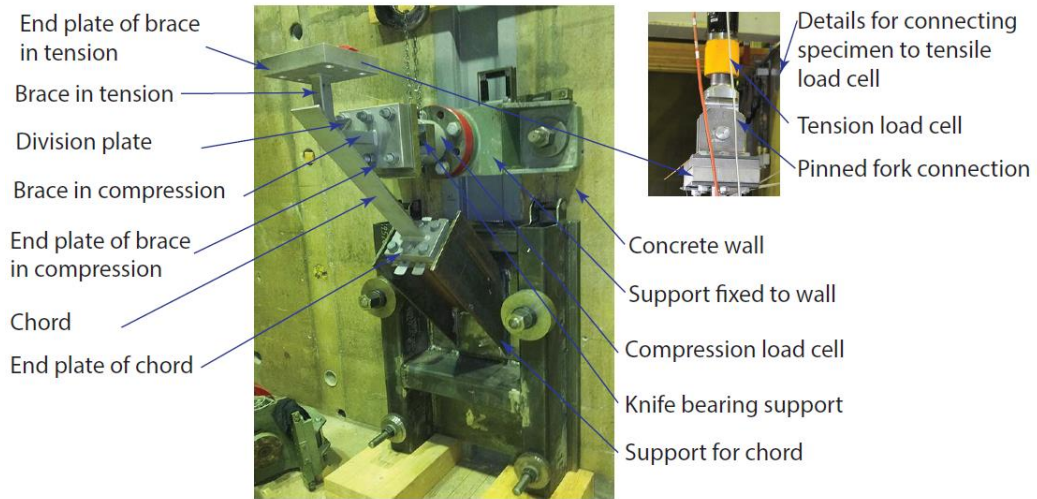

Figure 2. Details of specimen and test setup.

Table 1. Nominal and measured mechanical properties of steel used for joint members.

Member	Steel grade	Thickness [mm]	R_{eh} [N/mm^2]	R_m [N/mm^2]	Strain at fracture ε_u [mm/mm]
Bracings (tube)	S355J2H/ S420 MH	2.6	546.64	589.21	16.23%
Nominal (tube)	S355J2H	$2 \leq t \leq 2.99$	355	510-680	20%
	S420MH	$2 \leq t \leq 12.5$	420	500-660	19%
Chord (plate)	S420	12	445.46	552.90	31.05%
Division plate	S420	8	468.82	559.08	30.16%
Nominal (plate)	S420	$7 \leq t \leq 16$	420	520-680	19%

The nominal and measured dimensions of the specimen are listed in Table 2. The designation of the fabricated specimen is interpreted as follows: the first letter "J" represents Joint; the second letter followed by three digital numbers represents strength of the material; and the last letter represents the sequence of the tested joint. The symbols of b_0, t_0, and L_0 represent width, thickness, and length of the chord, respectively. Similarly, the symbols of b_i, t_i, L_i, and θ_i represent the width, the thickness, the length, and the inclination of the braces, respectively. Because the joint specimens were delivered as ready-made, the measured dimensions are all approximate values.

Table 2. Nominal and measured dimensions of the specimens in mm.

Specimen	Chord $b_0 \times t_0 \times L_0$	Bracings $b_i \times t_i \times L_i \times \theta$		Division plate $L_p \times h_p \times t_p$
		Tension	Compression	
Nominal	$104 \times 12 \times 630$	$40 \times 3 \times 200 \times 45$	$40 \times 3 \times 200 \times 45$	$100 \times 60 \times 8$
JS420-A	--	$40.3 \times 2.7 \times 200 \times 43.5$	$40 \times 2.7 \times 200 \times 45.75$	--
JS420-B	$104.4 \times 12.06 \times 630$	$40.3 \times 2.7 \times 200 \times 44.9$	$40 \times 2.7 \times 200 \times 43.08$	$100 \times 60 \times 8.08$
JS420-C	$104.2 \times 12.04 \times 630$	$40.3 \times 2.7 \times 200 \times 44.8$	$40 \times 2.7 \times 200 \times 43.8$	$100 \times 60 \times 8.04$
JS420-D	$104.1 \times 12.07 \times 630$	$40.3 \times 2.7 \times 200 \times 46$	$40 \times 2.7 \times 200 \times 43.7$	$100 \times 60 \times 8.01$

Experimental tests

The test setup were designed according to the studies performed in [7]. Figure 2 also shows details of the test arrangement. The test setup is aligned vertically to a reinforced-concrete reaction wall. The test specimen is connected to the tension load cell via a pinned support. A tensile load is transferred through an actuator to the tension brace of the specimen. The compression brace of the specimen rests on a knife bearing support. The reaction force to the compression brace is measured by the compression load cell that is fixed to the concrete wall by fixing bolts. The chord of the specimen is fixed to the chord support through the endplate of the chord. The tensile load to the chord is transferred through the support to the concrete wall. The load transferred to the chord member is determined from the strain values measured by strain gauges.

Four strain gauges were set on the chord and their locations are shown in Figure 3 (b). The strain gauges 1 and 2 were located on the top and the bottom surfaces of the chord, the strain gauges 3 and 4 were on the two sides of the chord, respectively. The strain gauges are 150 mm away from the surface of endplate of the chord. Since the chord remained in the elastic range during the loading, the measured elongations can be converted into force values based on the Hook's law.

The load-displacement curves obtained from the tests. The corresponding relative displacement of the tension or compression brace to the chord are measured by four Linear Variable Displacement Transducers (LVDTs). The plan of these LVDTs (S-7 to S-10) is shown in Figure 3 (b). The LVDT is attached to each side of the corresponding brace. One end of each LVDT is attached to the point at the mid-length of the corresponding brace, and the other end to the intersection point of the mid-lines of chord and division plate.

The out-of-plane displacements of the specimen were monitored by three other LVDTs (S-1 to S-3) that are attached to the endplate of the braces. Two of them were attached to the tension brace and one to the compression brace. One LVDT (S-6) was attached to the chord endplate to measure the possible longitudinal movement of the chord

support during the loading procedure. Two LVDTs (S-4 and S-5) were attached to the bottom surface of chord to measure its bending and twisting displacements. After the first test for the specimen JS420-A, two extra LVDTs (S11 and S12) were added for the specimen JS420-B to JS420-D. Two separate supports on each side of the specimen were needed to fix all the LVDTs used in all tests. The plan for all the LVDTs is shown in Figure 3. Besides the four strain gauges on the chord, other 32 gauges were used on specimen JS420-B in order to provide enough data to validate the FE models. The strain gauges for measuring axial strains are type of KFGS-5-120-C1. The grid length is 5 mm with strain limit of 5% percent.

During the test, the specimen was firstly loaded up to 50 kN or 80 kN and unloaded to zero to check the functionality of the test setup. After that, the specimen was reloaded up to around 150 kN (200 kN in the first test) with the loading rate of 5 kN/min. Then, the specimen was loaded up to failure as a displacement-controlled procedure. In order to reduce the oscillations of a load-displacement curve, the displacement rate in the displacement-controlled procedure was adjusted according to the observed shape of the load-displacement curve. By switching from a load-controlled procedure to a displacement-controlled one, the local buckling of the compressed brace can be followed. The test was stopped when the load applied to the joint was about 10% of the maximum load taken by the joint.
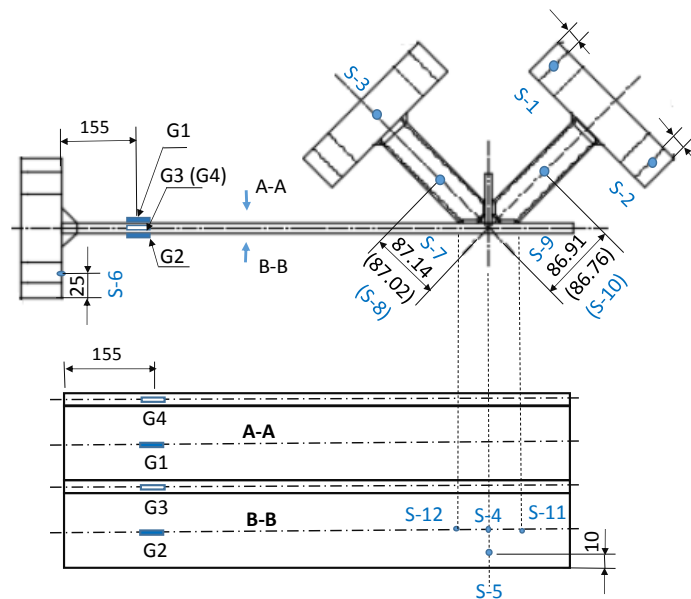

Figure 3. Plans for locating LVDT and strain gauges. (S1-S12 represent LVDTs. The unit of the dimensions to indicate locations of S1-S12 is in mm. G1-G4 represents the strain gauges attached to the chord.)

Results of joint tests

Deformation modes of the specimens

The global deformation modes of the specimens are shown in Figure 4 (a). The detailed views of the deformation modes of specimen JS420-C and specimen JS420-D are shown in Figure 4 (b) and (c), respectively. The failure of four tested specimens are all initiated by the local buckling on the wall surface of the compression brace facing to the chord. However, the locations initiating the local buckling are varied. For the specimens JS420-B and JS420-C, the local buckling initiated close to the joint side; for the specimens JS420-A and JS420-D, the local buckling initiated close to the endplate of compression brace.

(a)   (d)

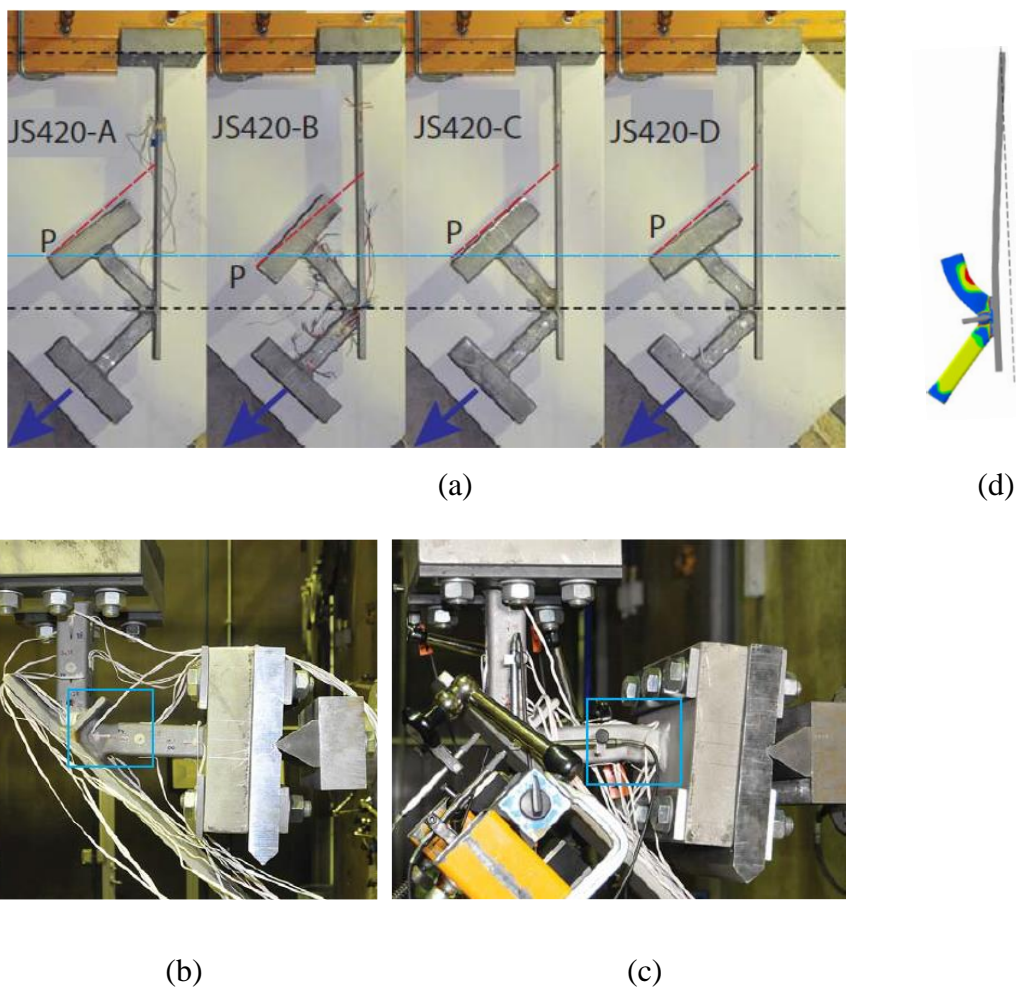(b)   (c)

Figure 4. Deformation modes of the scaled-down, isolated joint from tests and from FE analysis (a) deformation modes summarised from tests (b) detailed view for specimen JS420-C, (c) detailed view for specimen JS420-D (d) deformation mode from FE analysis

The maximum load was reached when the compressed brace buckled globally in the specimens JS420-A, JS420-B, and JS420-D. For the specimen JS420-C, the maximum

load of the joint was reached when the local buckling of the other three faces occurs at the location of the initiation of the local buckling. After reaching the maximum load, specimens JS420-A and JS420-D deformed by a uniaxial bending of the compression brace; specimen JS420-B had two-axial bending of the compression brace; and specimen JS420-C failed by the local crushing near the joint. The differences of the final deformation mode of the joint can be observed by the relative rotation of the endplate compared to the red lines shown in Figure 4 (a). It seems that the deformation mode of the joint is sensitive to the imperfections that may arise from assembly and manufacturing of the test specimens.

Load bearing capacity of the tested joint

Figure 5 shows load-displacement curves measured from two sides of each brace for the specimen JS420-A. When two curves for tension braces are compared, it can be seen that both curves have similar trends and reach the similar values of maximum load. However, the displacement measured from one side is larger than that measured from the other side. Similar behaviour has been observed for the two load-displacement curves measured from the compression brace. The difference between the displacements measured on two sides of the brace is caused by the out-of-plane movement of the bracings. The out-of-plane displacement is caused by the imperfections during the manufacture and the installation of the joint. For the further comparisons, the average of the two curves for each brace are calculated as shown in Figure 5.
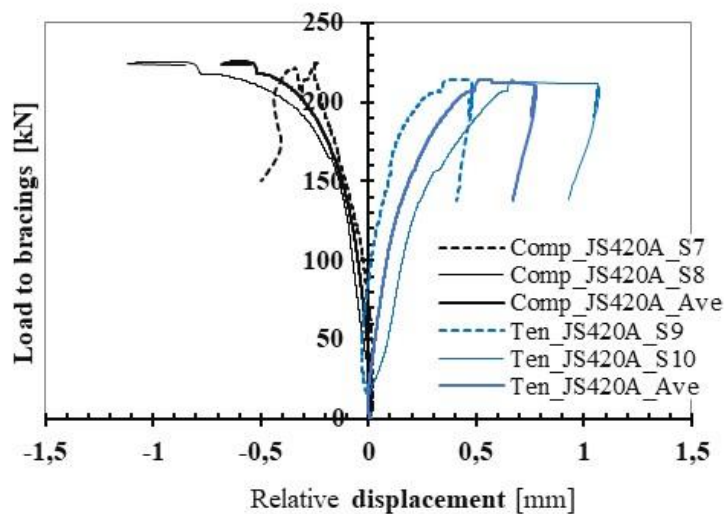

Figure 5. Load-displacement curves measured from two braces for specimen JS420-A and average values calculated from both sides of each brace

When the curves received from four tests are compared, the Figure 6 shows that the curves for the compression brace have similar initial stiffness up to around 190 kN. After that, the curves become non-linear and the maximum load of around 220 kN is reached in all cases. After reaching the maximum load, the curves deform differently: the curves for specimens JS420-A and JS420-D drop suddenly whereas the curves for specimens

44

JS420-B and JS420-C decrease gradually. These differences are caused by the different deformation modes observed in Figure 4, i.e. after the initiation of the local buckling in the compression brace, the compression braces of the specimens JS420-A and JS420-D buckle globally; the brace of the specimen JS420-B buckles in a double curvature; and the brace of the specimen JS420-C further buckles locally in other surfaces. With all the specimens tested, the tensile braces have similar load-displacement curves in terms of the initial stiffness and the maximum load bearing capacity.
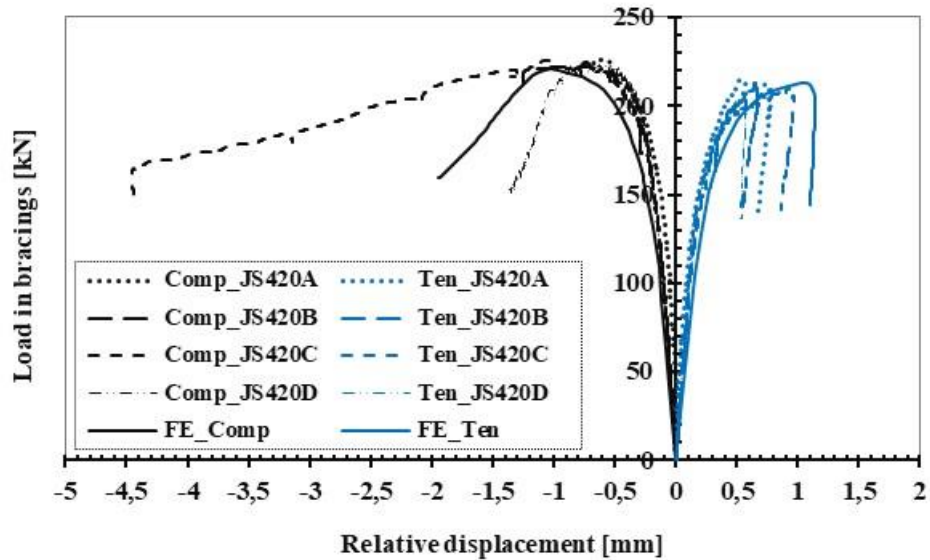

Figure 6. Load-displacement curves calculated as average values of displacement measured from two sides of tension or compression brace for the four specimens.

When the curve measured from the brace in tension is compared with that measured from the brace in compression for the same sample, it can be seen that the tensile brace enters the non-linear range earlier than the compressive brace, and the maximum load taken by the tensile brace is slightly lower than that taken by the compressive brace. From the same figure, it can be seen that the unloading of the tension brace is caused by the corresponding final buckling modes of the braces in compression. Figure 6 also shows that the displacements corresponding to the maximum loads on the compressive braces are between 0.8 mm and 1 mm; whereas those corresponding to the maximum load on the tensile braces are between 0.4 mm and 0.8 mm.

Load transferred from braces to chord

Figure 7 (a) shows the measured strains that are used to calculate the load transferred to the chord from braces for the specimen JS420-D. It can be seen from Figure 7 (a) that up to load values of 80 kN, the strains measured by strain gauges 2 and 4 are close to each other, and those measured by strain gauges 1 and 3 are close to each other. This feature originates from the installation tolerances which initiate twisting in the specimens. After yielding occurred in the surfaces of the brace close to the joint side, the initial twisting

45

was released. The two braces of the joint deforms more in the way of in-plane bending. Because of the intention to create both a simultaneous loading on braces in compression and in tension and a pinned support condition at the end of the chord, the length of the chord were extended. The extension of the chord length enhances the in-plane bending of the joint. Therefore, the release of the twisting increases the deviation of strain gauge 3 from strain gauge 1, and that of strain gauge 4 from strain gauge 2. The in-plane bending of two braces makes the strains measured by strain gauge 1 lower than those measured by strain gauge 2. Nevertheless, Figure 7 (b) shows that the load calculated based on the average values of measured strains correlates well with the load derived from the loads measured from tension and compression braces. The good fit between load values proves that the load was properly transferred inside the joint from the braces to the chord.
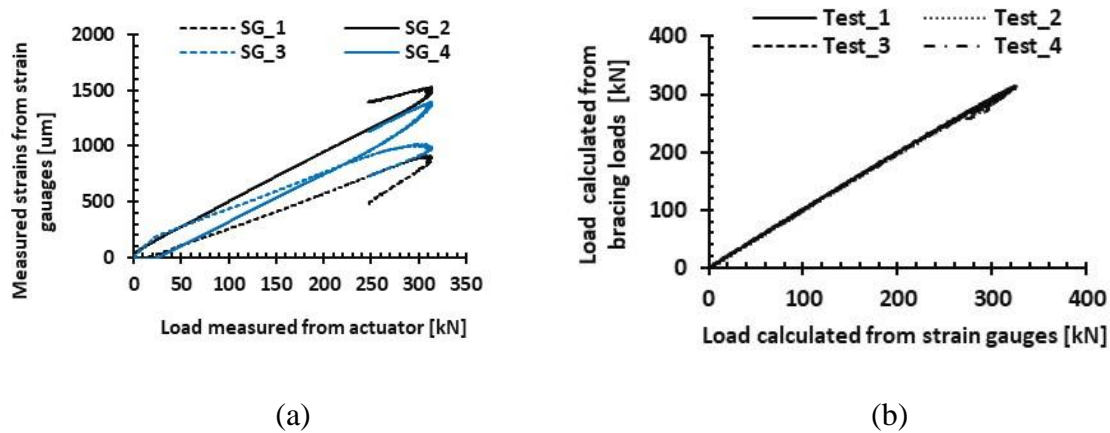

Figure 7. Load transferred from braces to the chord (a) strains measured by strain gauges installed on the chord in the specimen JS420-D (b) comparisons of the load calculated using measured strains with the load derived from the loads measured from tension and compression braces for the four specimens.

Out-of-plane displacements of the tested joint

Figure 8 (a) and (b) show how the measured out-of-plane displacements of the end plates of the braces varied with loads, and how the measured axial displacements relative to the fixing base of the chord varied with load for specimen S420-C, respectively. The LVDTs are attached to the endplates of two braces and to the endplate of the chord as shown in Figure 3 (b). As it can be seen from Figure 8 (a), the out-of-plane displacements measured from the endplates of both braces vary with the load in a similar way. The values of the out-of-plane displacement are increased with the increase of the load up to 50 kN. After that, the out-of-displacements remain constant. When the load reaches about 100 kN, the out-of-plane displacement starts to decrease until the maximum load is reached. It can be concluded that in the test the out-of-plane displacements increase until the initial yielding occurs inside the joint. The maximum value of the out-of-plane displacement in compression brace is about 0.4 mm and is about 2 mm in tension brace.

Figure 8 (b) shows that the axial displacement of the chord in relation to its fixing base (S_6_End_Axial) is close to zero up to the chord load of 150 kN, and increases to

0.2 mm up to the maximum load. It can be concluded that the specimen is fixed to this support properly. Figure 8 (b) also shows the variations of the out-of-plane displacement measured from the chord under two braces. As shown in Figure 3 (b), the LVDTs of S4 and S5 are located at the centre and the edge of the division plate, respectively; the LVDT of S11 is underneath of the tension brace; the LVDT of S12 is underneath the compression brace. S11 and S12 are located at the same line as S4. The measured displacements by S11, S12, and S6 relative to that measured by S4 show that the joint deforms as designed.

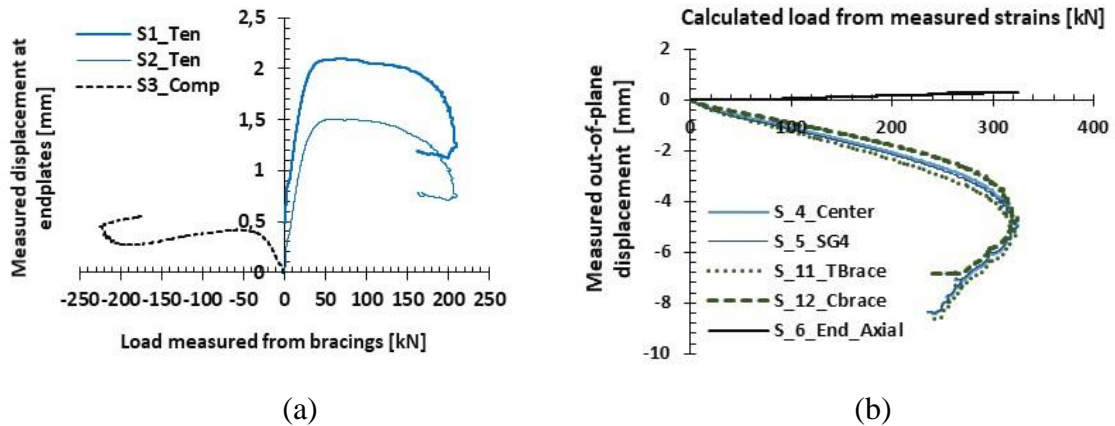(a)   (b)

Figure 8. Variations of measured displacements at endplates of both bracings and chord with their corresponding loads for specimen JS420-C (a) displacements measured on bracings (b) displacements measured on chord.

Comparisons and discussions

In this section, the load-carrying capacity of the tested joint is firstly used to validate the FE model created for the tested joint. After that, the validated FE model is modified by using boundary conditions close to the real joint. The material model is defined using both measured and nominal material properties. The results are then up-scaled and compared with the results obtained from the FE models created for both the full-scale joint and the joint inside the truss. The purpose of the comparisons is to evaluate the accuracy of FE models created for the full-scale joint. Figures 9 (a), (b), (c) and (d) show the joint models selected for the comparisons.

   The joint in Figure 9 (a) is the tested joint. Figure 9 (b) shows the FE model created in [7] for the tested joint. In the model, the load is applied to the brace in tension. Pinned boundary condition is assigned to the end of the two braces, while fixed boundary condition is assigned to the end of the chord. Based on the studies in [7], the length of the chord is determined numerically as 5 times of the width of the chord. With this length of the chord, the joint with a fixed end of the chord behaves similarly to the joint with a chord length of four times the chord width and a pinned end of the chord. To account for the inward horizontal movement of the load cell during the tests, a horizontal movement predefined is applied at the end of the tension brace. The model shown in Figure 9 (c) is the FE model created for the full-scale, isolated joint in [7], [8]. The symmetry of the joint

has been utilized. All the FE analyses have been carried out using Abaqus/standard and more details for creating the models can be found in [5], [7], [8].
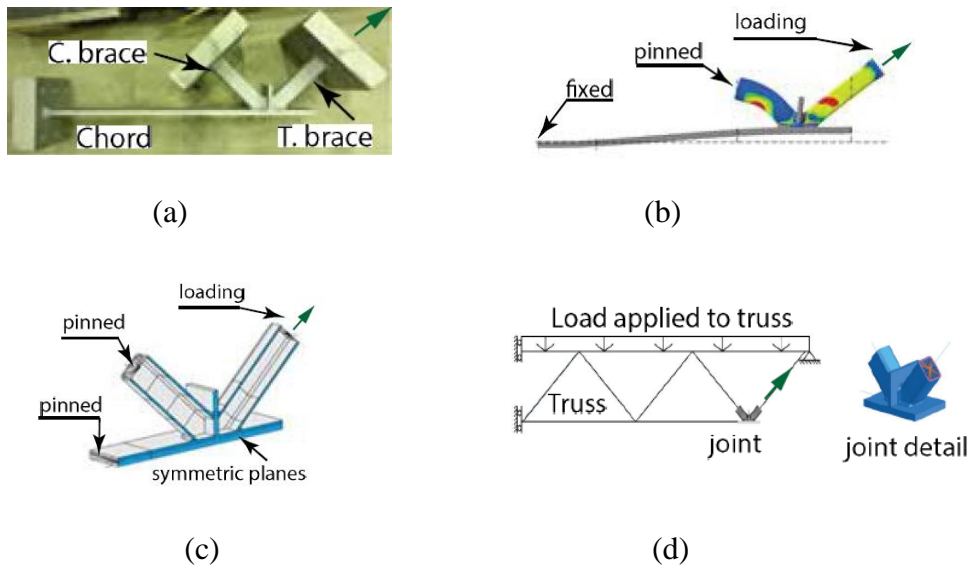

(a)

(b)

(c)

(d)

Figure 9. Joint models selected for the comparisons (a) tested joint (b) scaled-down isolated joint model (FE) [7] (c) full-scale isolated joint model (FE) [8] (d) full-scale truss-joint model [5].

Validation of FE model created for the tested joint

The FE model created for the tested joint is validated by comparing results between FE analyses and tests. As shown in Figure 4, when the deformation modes of the joint from all four tests are compared to that of the joint from the scaled-down, isolated model in FE analyses, it can be seen that the local buckling occurred on the surface of compressive bracing in all cases. However, the locations of initiating the local buckling varied. Both the specimen JS420-A and the specimen JS420-D buckle locally at the similar locations to the joint predicted by FE analyses. As discussed in the previous sections, after the local buckling occurred, the specimen JS420-A, JS420-B, and JS420-D buckled globally. It seems that the specimen JS420-D has the deformation mode that is the closest with the mode predicted by FE analyses for the isolated joint model.

The load – displacement curves of joint received from the tests and those calculated by FE models are shown in Figure 6. In the FE analyses, the material model was created with measured material properties. It can be seen that the curves from FE analyses have similar trends to those from tests. The initial linear and non-linear parts overlap each other. The unloading in the load –displacement curve for tension brace comes from the buckling failure of brace in compression. The buckling of brace in compression prevents the brace in tension from deforming further. When the load capacity of the joint is compared, the value obtained from tests is about 2–5% lower than that obtained from FE analyses. The displacements at maximum load predicted by FE analyses for the compressive brace are in the middle of those obtained from tests. The displacements predicted by FE analyses for the tension brace are close to those obtained for the specimen

48

S420D but much higher than those obtained for other specimens. The maximum loads reached and their corresponding displacements are summarised in Table 3.

During the installation, the joint is aligned to the load cell attached to the brace in compression, therefore, the variation of measured displacements observed from the tension brace is large. Since the strength degradation of the joint is controlled by the failure of the compression brace, the displacements measured from the tensile brace are used only for control purpose. The comparisons of other values in Table 3 show that the FE model developed for the scaled-down, isolated joint model predicts the test results well. The modelling method can be further applied to validate model created for the scaled-down model with similar dimensions or the full-scale joint.

Table 3. Comparisons of load capacity and the maximum displacement for scaled-down joint between tests and FE analyses.

Methods	Joint-types	Maximum load in bracings [kN]		Displacements at maximum load [mm]	
		Tension	Compression	Tension	Compression
Test (scaled-down)	JS420-Ave-SD-Iso-Test (1)	210.06	222.19	--	--
	JS420-C-SD-Iso-Test (2)	210.45	225.63	0.93	1.05
	JS420-D-SD-Iso-Test (3)	204.96	223.62	0.56	0.66
FEA (scaled-down similar to test conditions)	JS420-SD-Iso-FE-Real (4)	212.78	220.60	1.07	1.02
FEA/Test (scaled-down)	(4) / (1)	1.01	0.99	--	--
	(4) / (2)	1.01	0.98	1.15	0.97
	(4) / (3)	1.04	0.99	1.91	1.55

Evaluation of FE models created for full-scale joint

When scale factors used for dimensioning the specimens are evaluated using the validated simulation method, the load-bearing capacity and the displacement of the scaled-down joint predicted numerically are multiplied by the corresponding scaling factors of 11.97 and 3.46 determined in [7]. The up-scaled results are compared with those predicted by FE models for both full-scale, isolated joint and the joint inside the truss. The comparison of the results is shown in Table 4. Since specimens tested are initially dimensioned based on FE models using nominal material properties, Table 4 lists the results for the scaled-down joint modelled using nominal material properties. The symbols to designate the type of the joint in Table 4 can be read as follows: Joint (J), Steel grade (S420), size of the

joint (scaled-down, scaled up, or full-scale joint), joint type (isolated-joint model or truss-joint model), study method (FE analysis), and material models in FE analysis (measured value, "Real", or nominal value, "Norm"). For instance, "JS420-FS-Iso-FE-Real" can be read as: Joint – Steel grade S420 – Full scale – isolated joint – FE using measured material properties.

When the maximum load reached in the corresponding braces are compared, it can be seen that the values obtained from both full-scale joint model and truss-joint model are very close to their corresponding values up-scaled from the scaled-down model. The ratios vary from 0.92 to 0.95. When the displacements are compared, the values of the compression brace predicted by full-scale models vary from 0.95 to 1.10 times of the values up-scaled from the results of the scale-down joint model. However, for the braces in tension, the discrepancy is larger. Further analyses in the future would be useful even if the tension brace is not limiting the load-bearing capacity in this case.

Table 4. Verification of the scale factors by comparing both load and displacement received from full scale joints using various FE models.

Methods	Joint-types	Max. load in bracings [kN]		Displacement at max. load [mm]	
		Tension	Compression	Tension	Compression
Scaled-down-FEA	JS420-SD-Iso-FE-Norm (6)	231	243	3.5	2.1
Up-scaled from scaled-down-FEA	JS420-FS-Iso-FE-Norm (7)	2765 (6)x11.97	2909 (6)x11.97	12.11 (6)x3.46	7.3 (6)x3.46
Full-scale-FE-Iso	JS420-FS-Iso-FE-Norm (8)	2617	2690	$\cong$9.4	$\cong$7.0
Full-scale-FE-Truss	JS420-FS-Truss-FE-Norm (9)	$\cong$2600	$\cong$2700	$\cong$8	$\cong$8
Comparisons among methods	(8) / (7)	0.95	0.92	0.77	0.95
	(9) / (7)	0.94	0.93	0.66	1.10

Conclusions and future researches

The load-displacement curves obtained from the experimental tests show that the stiffness and the strength of the four tested specimens are similar but the displacements at maximum load vary. The failure of the joint is initiated by the local buckling of the brace in compression. However, the locations of the initiation of the deformation mode leading to the failure of the joint are specimen dependant. In addition, the maximum values of the load reached in the compression brace and in the tension brace were different in the tests. This difference is caused by the out-of-plane displacements of the endplate of the tension brace, which is confirmed by simulating a lateral movement of the endplate of the tension

brace by the FE models. It seems that both variations of failure modes and out-of-plane displacements observed in tests are caused by the imperfections of the joint specimens. This highlight the importance to control tolerances during the manufacturing and assembly process.

The load-displacement curves obtained from FE analyses performed on the scaled-down, isolated joint coincide reasonably with experimental results in terms of the initial stiffness and the maximum load capacity. In addition, the displacements at maximum loads predicted from FE models are close to the displacements measured in some tests. Overall, it can be concluded that the modelling method used in FE analyses are validated by the test results and can be applied further to investigate the behaviour of the similar type of joint.

The upscaling of the results of the scaled-down, isolated joint shows that the load-carrying capacity received for the joint is very close to those predicted by FE analyses using both full-scale, isolated joint and truss-joint models. Therefore, it can be concluded that the technique of performing the tests on the scale-down specimen offers opportunities to test members and joints made of high strength steel by devices without extremely high force output.

Acknowledgement

References

[1]   Y. Chen, R. Feng, L.Q. Fu, Investigation of grounted stainless steel SHS tubular X- and T-joints subjected to axial compression. *Engineering Structures,* 150: 318–333, 2017. https://doi.org/10.1016/j.engstruct.2017.07.052

[2]   Y.S. Choo, X.D. Qian, J.Y.R. Liew, J. Wardenier, Static strength of thick-walled CHS X-joints—Part I. New approach in strength definition. *Journal of Constructional Steel Research,* 59(10): 1201–1228, 2003. https://doi.org/10.1016/S0143-974X(03)00054-3.

[3]   EN1993-1-8, Eurocode 3: design of steel structures - Part 1-8: design of joints, European Committee for Standardization, 2005.

[4]   A. Jurmu, *The Basis of Design of The WQ-Lattice Bottom Chord Joint.* The University of Oulu, Oulu, Finland, 2011.

[5]   J. Kadak, *Effect of steel strength on the welded joint between a plate and two tubular cross-sections.* Master's thesis. Aalto University, Espoo, 2014.

[6]   J.A. Packer, J. Wardenier, X.L. Zhao, G.J. van der Vegte, Y. Korubane, *CIDECT Design Guide 3: for Rectangular Hollow Section (RHS) Joints under Predominantly Static Loading*. CIDECT, 2009.

[7]   P. Saremi, *Numercial design of experimental set-up for a welded K-joint of a long-span truss.* Master's thesis. Aalto University, Department of Civil Engineering, Espoo, 2016.

[8]   P. Saremi, W. Lu, J. Puttonen, J. Kadak, Investigation of welded K-type joints inside floor truss system. in *8th International Conference on Steel and Aluminium Structures*. Hong Kong, China, 2016.

[9]   SFS-EN10025-4, Hot Rolled Products of Structural Steels. Part 4: Technical Delivery Conditions for Thermomechanical Rolled Weldable Fine-grain Structural Steels, 2005.

[10] SFS-EN10219-1 Cold-formed welded structural sections of non-alloy and fine grain steels Part 1: Technical delivery conditions, 2006.

[11] SFS-EN10219-2 Cold-formed welded structural hollow sections of non-alloy and fine grain steels. Part 2: tolerances, dimensions, and sectional properties, 2006.

[12] SSAB, SSAB Comex Tube Double Grade. https://www.ssab.fi/tuotteet/terasluokat/rakenneputket/tuotteet/ssab-domex-tube-double-grade, 2017.

[13] B. Young, K.J.R. Rasmussen, Stainless steel tubular joints - tests and design of X- and K-joints in square hollow sections. in *12th International Specialty Conference on Cold-Formed Steel Structures*, Saint Louis, Missouri, U.S.A, 1994.

Pooya Saremi, Wei Lu, Jari Puttonen
Department of Civil Engineering, Aalto University
00076 AALTO
pooya.2.saremi@aalto.fi, wei.2.lu@aalto.fi, jari.puttonen@aalto.fi

Dan Pada, Jyrki Kesti
Ruukki Construction Oy, SSAB
dan.pada@ruukki.com, jyrki.kesti@ruukki.com